Journal of Computational and Applied Mathematics 246 (2013) 65–73

Contents lists available at SciVerse ScienceDirect

Journal of Computational and Applied Mathematics

journal homepage: www.elsevier.com/locate/cam

A multiscale domain decomposition approach for chemical vapor deposition

J. Bogers [a], K. Kumar [a,*], P.H.L. Notten [b], J.F.M. Oudenhoven [c], I.S. Pop [a,d]

[a] CASA, Department of Mathematics and Computer Sciences, Technische Universiteit Eindhoven, 5600 MB, Den Dolech2, Eindhoven, Netherlands

[b] EMD, Department of Chemical Engineering, Technische Universiteit Eindhoven, 5600 MB, Den Dolech2, Eindhoven, Netherlands

[c] imec/Holst Center, P.O. Box 8550, 5605 KN Eindhoven, Netherlands

[d] Institute of Mathematics, Johannes Bruns Gt. 12, University of Bergen, Norway

ARTICLE INFO

Article history:
Received 27 January 2012
Received in revised form 17 September 2012

Keywords:
Domain decomposition
Reactive flows
Chemical vapor deposition
Multiscale

ABSTRACT

We consider the process of chemical vapor deposition on a trenched Si substrate. To understand the process (including e.g. the layer conformality) at the trench scale (*microscale*), we need solutions at both the trench and reactor scales (*macroscale*). Due to the huge difference in size of these scales, straightforward numerical computations are very challenging. To overcome this difficulty, we consider a multiscale approach by introducing an intermediate scale (the *mesoscale*). We start with a time-continuous model describing the transport processes and then perform time discretization. At each time step, using the ideas of domain decomposition inspired from Lions (1988) [4], we provide iterative coupling conditions for these three different scales. Using a weak formulation for the time-discrete equations, we prove the convergence of this iterative scheme at each time step. The approach also provides an alternative proof for the existence of the solutions for the time-discrete formulation.

1. The motivation

This work is motivated by the chemical vapor deposition (CVD) processes involved in the manufacturing of 3D all-solid-state batteries. In such a process, a carrier gas flows through a tube with rectangular cross-section (the reactor). A silicon (Si) substrate is placed at the bottom of the reactor. The carrier gas transports small amounts of reactive substances, the precursors. These precursors react at the substrate, which becomes the lower part of the reactor boundary, where a solid layer is produced [1–3]. This leads to an overall transport process with reactions at the boundary. The details of the mathematical models are provided in Section 3.

To increase the energy storage capacity of the batteries, the geometry of the Si substrate is made complex. To increase the surface area, trenches are etched in the Si substrate, which therefore has a rough surface instead of being flat. The typical size of a trench is of the order of micrometers ($\sim 10\,\mu$m), whereas the substrate size is of the order of ~ 30 cm. This evidently indicates the existence of two distinct scales in the problem: the trench scale (referred to as the *microscale*) and the reactor scale (the *macroscale*).

For a thorough understanding of the CVD process, and in particular the conformality of the deposited layers, one needs an accurate computation of the solution at the trench scale. However, this requires computing the solution at the reactor scale as well. The scale difference (an order of $\sim 10^4$) makes a direct numerical simulation computationally demanding because

* Corresponding author. Tel.: +31 641224384.
E-mail addresses: j.j.p.bogers@student.tue.nl (J. Bogers), k.kumar@tue.nl, k.kundan@gmail.com (K. Kumar), p.h.l.notten@tue.nl (P.H.L. Notten), jos.oudenhoven@imec-nl.nl (J.F.M. Oudenhoven), i.pop@tue.nl (I.S. Pop).

0377-0427/$ – see front matter © 2012 Elsevier B.V. All rights reserved.
doi:10.1016/j.cam.2012.10.018

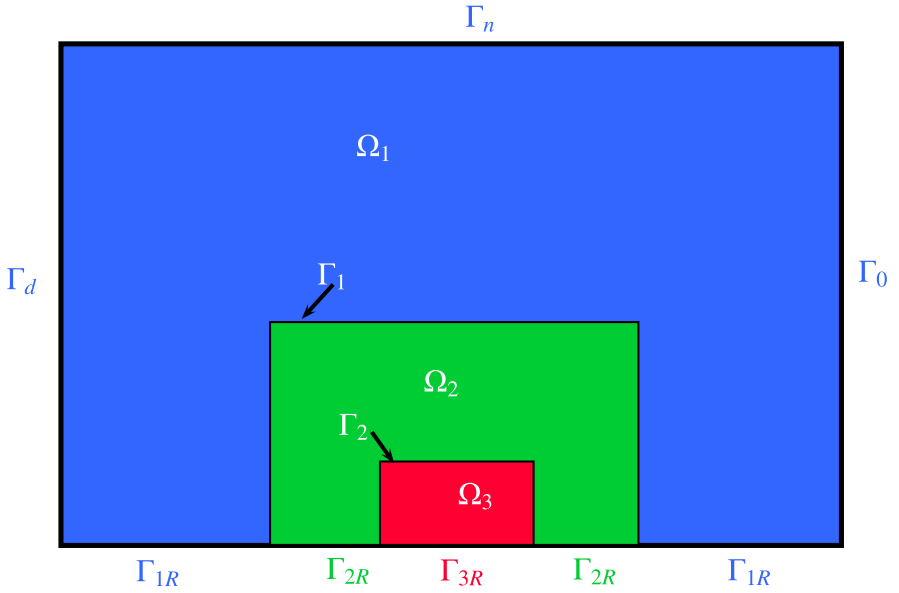

Fig. 1. Schematic for the multiscale computation method.

of the very fine mesh required for resolving the trench scale. Alternatively, we can zoom in on a small region of the reactor near the region of interest, the substrate. This introduces an intermediate scale, henceforth referred to as the *mesoscale*. Next we zoom in on a small region of the mesoscale where the trenches (the microscale) can be identified. These three domains are thus formed as a result of successive zooming in, so the trenches are resolved only at the microscale, and the mesoscale is used only for exchanging the information from the macroscale to the microscale. To compute the solution at each scale, conditions of coupling between the different scales are needed. In doing this, we use ideas from the domain decomposition method.

Our aim here is to provide a numerical scheme allowing us to compute the detailed solutions at each scale. The focus being on the numerics for the transport equations, we consider a simple flow model, allowing a complete decoupling from the transport equations. Moreover, the flow is computed only at the macroscale and projected further at the mesoscale. However, the transport equations describing the concentration of the reactants (precursor) are defined for all the three scales. The coupling between different scales is through the boundary conditions providing the continuity of the concentration and that of the normal fluxes. To achieve this, we first perform the time discretization of the model. Then, at each time step, an iterative non-overlapping domain decomposition algorithm [4] is considered. The iteration involves a linear combination of the normal fluxes and the concentrations at the separating boundaries, allowing a decoupling of the models at the different scales. For the iterative scheme, rigorous convergence results are obtained by compactness arguments. This approach allows a comparison of the numerical results with the experimental results, and identifying parameters such as the diffusion coefficient and the reaction rate constants for the deposition process. This can hence be used to predict the deposition under alternative conditions and also for different geometries.

Below we briefly describe the geometry in Section 2 and provide the mathematical model in Section 3. In Section 4, we give the definitions of the weak solutions for both the time-continuous and the time-discrete equations. Next, the iterative non-overlapping domain decomposition algorithm is considered. This is followed by the proof of convergence of this iterative numerical method.

2. The mathematical model

In this section we give a simplified mathematical model for the motivating application. This model describes the reactive flow inside a reactor, with reactions taking place on the substrate which is a part of the boundary. Before giving the equations we give some details regarding the geometry of the system, justifying the multiscale approach. The scales introduced above (macroscale, mesoscale and microscale) involve three domains, Ω_1, Ω_2 and Ω_3. Their boundaries are denoted by $\partial\Omega_j$, $j = 1, 2, 3$, respectively. Each boundary $\partial\Omega_j$ includes a part Γ_{jR} where reactions (depositions) take place. For the other parts of boundaries, let us first consider the microscale. We define $\Gamma_2 = \partial\Omega_3 \setminus \Gamma_{3R}$, where the variables in Ω_2 and Ω_3 are coupled. For the mesoscale, we define two parts of $\partial\Omega_2$, namely, Γ_1 and Γ_2. These provide the coupling with Ω_3 and Ω_1, respectively. In other words, $\Gamma_2 = \partial\Omega_3 \cap \partial\Omega_2$ (the interface between the microscale and the mesoscale), while $\Gamma_1 = \partial\Omega_1 \cap \partial\Omega_2$ (the interface between the macroscale and the mesoscale). Fig. 1 displays these regions and the nomenclature.

3. The equations

The mathematical model consists of two components: the flow and the reactive transport. The reactive substance (precursor) is transported to the substrate through a combined effect of convective flow and the molecular diffusion. The flow velocity of the carrier gas is described by the Navier–Stokes system, while the reactive transport processes are described by the linear convection–diffusion equation.

3.1. The flow component

The focus here is on the numerics for the reactive transport component. For the flow we consider a simplified setting, allowing a decoupling from the transport part. For instance, thermal effects are disregarded. Next, as suggested by the numerical evidence, the flow is absent in the trenches and therefore the flow is considered only at the macroscale and the mesoscale, where no roughness is encountered at the boundary. Further simplifications include that the flow is laminar and incompressible, and no gravity effects are taken into account. It is also assumed that the concentration of the precursor is much smaller than that of the carrier gas and, hence, the flow is not affected by the adsorption of the precursors. Finally, we only consider a steady state; hence the flow problem needs to be solved only once (at the beginning). Under the above assumptions, the flow component of the model reads

$$\begin{aligned} &\text{Continuity: } \nabla \cdot \mathbf{q} = 0, \\ &\text{Momentum: } \rho \mathbf{q} \cdot \nabla \mathbf{q} = \nabla \cdot \left(\mu(\nabla \mathbf{q} + \nabla \mathbf{q}^T) - \mu(\nabla \cdot \mathbf{q})I\right) - \nabla P, \end{aligned} \tag{3.1}$$

in the simple domain $\Omega_1 \cup \Omega_2 \cup \Gamma_1$, where $\mathbf{q}$ is the gas velocity and P its pressure. For the boundary conditions, we provide a parabolic inlet for the velocity (at Γ_i) and use no-slip boundary conditions at the side walls. We prescribe pressure at the outlet Γ_o.

$$\mathbf{q} = \mathbf{q}_d \quad \text{on } \Gamma_d; \qquad P = P_0 \quad \text{on } \Gamma_o; \quad \text{and} \quad \mathbf{q} = 0 \quad \text{on } \Gamma_2 \cup \Gamma_{1R} \cup \Gamma_{2R} \cup \Gamma_n,$$

and, for instance, in 2D, the choice of parabolic inlet profile gives $\mathbf{q}_d = Q(\ell^2 - y^2)\mathbf{e}_1$, where Q is a positive constant and $\mathbf{e}_1$ is a unit vector along the x-direction.

3.2. The reactive transport/deposition equations

For the CVD model we restrict to the basic equations, including the convective transport and the molecular diffusion, neglect the reactions taking place in the gas phase and consider the situation where the precursor has only one species. Inside the domain Ω_i, its concentration is denoted by u_i, where $i = 1, 2, 3$ is indexing the scale. For the boundary conditions we assume that the deposition takes place only on the bottom plate (the substrate). For simplicity, we assume a first-order kinetics.

3.2.1. The macroscale equations

With $T > 0$ standing for the maximal time, at the reactor scale the precursor is modeled by the linear convection–diffusion equation

$$\partial_t u_1 - \Delta u_1 + \mathbf{q} \cdot \nabla u_1 = 0 \quad \text{in } \Omega_1 \times (0, T] \tag{3.2}$$

coupled with the reactive boundary conditions

$$-\boldsymbol{\nu} \cdot \nabla u_1 = C_R u_1 \quad \text{on } \Gamma_{1R} \times (0, T], \tag{3.3}$$

where C_R is the (positive) reaction constant. The macroscale equations are coupled with the microscale ones at $\Gamma_1 \subset \partial\Omega_1$. The boundary $\partial\Omega_1 = \Gamma_d \cup \Gamma_n \cup \Gamma_o \cup \Gamma_{1R} \cup \Gamma_1$ and the boundary part Γ_d has non-zero measure where Dirichlet boundary conditions are prescribed, and for $\Gamma_n \in \Gamma_o$ homogeneous Neumann boundary conditions ($-\boldsymbol{\nu} \cdot \nabla u_3 = 0$) are taken.

3.2.2. The mesoscale equations

At the mesoscale we use the same equation for the precursor:

$$\partial_t u_2 - \Delta u_2 + \mathbf{q} \cdot \nabla u_2 = 0 \quad \text{in } \Omega_2 \times (0, T] \tag{3.4}$$

and the reactive boundary conditions:

$$-\boldsymbol{\nu} \cdot \nabla u_2 = C_R u_2 \quad \text{on } \Gamma_{2R} \times (0, T]. \tag{3.5}$$

Coupling conditions are imposed along $\Gamma_2 \cup \Gamma_1$, as explained in the next section.

3.2.3. The microscale equations

The geometrical dimensions of the microscale are comparable to the mean free path length of the gas particles. This means that the diffusion is no longer Fickian, but involves the Knudsen diffusion coefficient, a parameter that can be determined by comparing with experimental results. Further, we ignore the convective term for the transport in the trench as the velocity is negligible. Also, the flux at the mesoscale automatically takes into account the flux due to convection. The deposition process inside the trench is described by the following equations:

$$\partial_t u_3 = D_T \Delta u_3 \quad \text{in } \Omega_3 \times (0, T] \tag{3.6}$$

where D_T is the diffusion coefficient, and outside the trench we use the Fickian diffusion while inside the trench we use a different diffusion coefficient. For the boundary conditions we prescribe

$$-\boldsymbol{\nu} \cdot \nabla u_3 = C_R u_3 \quad \text{on } \Gamma_{3R} \times (0, T] \tag{3.7}$$

where Γ_{3R} is the surface on which reactions take place. The remaining boundary part $\partial\Omega_3 \setminus \Gamma_{3R}$ is involved in the coupling with the mesoscale, as explained below.

Remark 3.1. Note that we have the same structure for the equations defined for the macroscale as well as the mesoscale. This is due to the fact that the ratio of microscale to macroscale is of the order 10^4 and a two-step domain decomposition algorithm would require very small discretization to allow coupling with the microscale boundaries. To overcome this discretization restriction, we propose a three-stage numerical scheme for computing the solution.

3.2.4. The coupling conditions

The different scales are coupled by the boundary conditions at non-reactive surfaces. We provide coupling conditions that are natural for this setting of the problem, namely, the flux continuity and the continuity of the concentrations. Specifically, after having fixed the normal $\boldsymbol{\nu}$ to Γ_1 and into Ω_1, we have the following coupling conditions:

$$\boldsymbol{\nu} \cdot (-\nabla u_2 + \mathbf{q} u_2) = \boldsymbol{\nu} \cdot (-\nabla u_1 + \mathbf{q} u_1) \quad \text{on } \Gamma_1 \tag{3.8}$$

and

$$u_1 = u_2 \quad \text{on } \Gamma_1. \tag{3.9}$$

Similar coupling conditions are imposed at the interface Γ_2 between the microscale and mesoscale:

$$u_2 = u_3 \quad \text{and} \quad \boldsymbol{\nu} \cdot (-\nabla u_2 + \mathbf{q} u_2) = -D_T \boldsymbol{\nu} \cdot \nabla u_3 \quad \text{on } \Gamma_2. \tag{3.10}$$

Having specified the boundary conditions, the model is closed by the initial conditions:

$$u_1(0, \cdot) = u_1^0, \qquad u_2(0, \cdot) = u_2^0, \qquad u_3(0, \cdot) = u_3^0. \tag{3.11}$$

For more general coupling conditions (transmission problems), we refer the reader to [5,6].

4. The numerical scheme

In this section we analyze the numerical scheme for solving the reactive transport model component problem, set up in the three subdomains of the reactor. The scheme is based on the Euler implicit time stepping. We start by defining the concept of weak solution for both the time-continuous and the time-discrete cases. Then, for the resulting sequence of time-discrete problems we give an iterative domain decomposition scheme, and prove its convergence on the basis of compactness arguments.

4.1. The weak form

We start with the concept of the weak solution for the coupled model in (3.2)–(3.11), using standard notation in the functional analysis. In particular, $H^1(\Omega_i)$ is the Sobolev space of functions defined on Ω_i and having L^2 weak derivatives. By $H^1_{0,\Gamma_D}(\Omega_i)$ we mean the function in $H^1(\Omega_i)$ having a vanishing trace on Γ_D, and $H^{-1}(\Omega_i)$ is its dual. Further, $L^2(0, T; X)$ is the Bochner space of functions valued in X, and $(\cdot, \cdot)_U$ denotes the inner product in $L^2(U)$ (with U a bounded domain) or the duality pairing between H^1_{0,Γ_D} and its dual. Finally we define the spaces

$$\mathcal{V}_i = \{u_i \in L^2(0, T; H^1_{0,\Gamma_D}(\Omega_i)) \mid \partial_t u_i \in L^2(0, T; H^{-1}(\Omega_i))\}, \quad i = 1, 2, \text{ or } 3.$$

Also, let $\Omega_i^T := \Omega_i \times (0, T)$, $\Gamma_{iR}^T = \Gamma_{iR} \times (0, T)$ and assume that $u_i^0 \in H^1_{0,\Gamma_D}(\Omega_i)$ for all i. Furthermore, for $\mathbf{q}$ we assume that $\mathbf{q} \in H(div; \Omega_1 \cup \Omega_2) \bigcap L^\infty(\Omega_1 \cup \Omega_2)$. Adopting the standard definition, $H(div; \Omega)$ consists of vector valued functions having divergence in $L^2(\Omega)$.

Definition 4.1. A weak solution of (3.2)–(3.11) is a triple $(u_1, u_2, u_3) \in \mathcal{V}_1 \times \mathcal{V}_2 \times \mathcal{V}_3$ satisfying the initial conditions $u_i(0, \cdot) = u_i^0$ ($i = 1, 2$, or 3), the boundary conditions

$$u_1 = u_2 \quad \text{at } \Gamma_1, \qquad u_2 = u_3 \quad \text{at } \Gamma_2,$$

and

$$\begin{aligned}&(\partial_t u_1, \phi_1)_{\Omega_1^T} + (\nabla u_1, \nabla \phi_1)_{\Omega_1^T} + (\boldsymbol{q}\nabla u_1, \phi_1)_{\Omega_1^T} + (C_R u_1, \phi_1)_{\Gamma_{1R}^T}\\ &\quad + (\partial_t u_2, \phi_2)_{\Omega_2^T} + (\nabla u_2, \nabla \phi_2)_{\Omega_2^T} + (\boldsymbol{q}\nabla u_2, \phi_2)_{\Omega_2^T} + (C_R u_2, \phi_2)_{\Gamma_{2R}^T}\\ &\quad + (\partial_t u_3, \phi_3)_{\Omega_3^T} + (D_T \nabla u_3, \nabla \phi_3)_{\Omega_3^T} + (C_R u_3, \phi_3)_{\Gamma_{3R}^T} = 0\end{aligned} \tag{4.1}$$

for all $\phi_i \in L^2(0, T; H^1_{0,\Gamma_D}(\Omega_i))$ such that $\phi_1 = \phi_2$ at Γ_1 and $\phi_2 = \phi_3$ at Γ_2.

In this section the equalities at the non-reactive interfaces Γ_1 and Γ_2 should be interpreted in the sense of traces. Next we consider the Euler implicit time discretization of (4.1). To this end we take $N \in \mathbb{N}$ and define $\triangle t = T/N$. With $t_k = k \triangle t$ and u_i^k approximating $u_i(t_k)$ ($i = 1, 2,$ or 3; $k = 1, \ldots, N$), the time-discrete solution triple at $t = t_k$ is defined by:

Definition 4.2. Given $u_i^{k-1} \in H^1_{0,\Gamma_D}(\Omega_i)$ we seek $u_i^k \in H^1_{0,\Gamma_D}(\Omega_i)$ satisfying

$$u_1^k = u_2^k \quad \text{at } \Gamma_1, \qquad u_2^k = u_3^k \quad \text{at } \Gamma_2,$$

and

$$\begin{aligned}&\frac{1}{\triangle t}(u_1^k - u_1^{k-1}, \phi_1) + (\nabla u_1^k, \nabla \phi_1) + (\boldsymbol{q}\nabla u_1^{k-1}, \phi_1) + (C_R u_1^k, \phi_1)_{\Gamma_{1R}}\\ &\quad + \frac{1}{\triangle t}(u_2^k - u_2^{k-1}, \phi_2) + (\nabla u_2^k, \nabla \phi_2) + (\boldsymbol{q}\nabla u_2^{k-1}, \phi_2) + (C_R u_2^k, \phi_2)_{\Gamma_{2R}}\\ &\quad + \frac{1}{\triangle t}(u_3^k - u_3^{k-1}, \phi_3) + (D_T \nabla u_3^k, \nabla \phi_3) + (C_R u_3^k, \phi_3)_{\Gamma_{3R}} = 0\end{aligned} \tag{4.2}$$

for all $\phi_i \in H^1_{0,\Gamma_D}(\Omega_i)$, such that $\phi_1 = \phi_2$on Γ_1 and $\phi_2 = \phi_3$ on Γ_2.

Note that in either the time-continuous case or the time-discrete one, the equations set up in each subdomain are coupled by imposing explicitly the continuity of the concentrations at the non-reactive surfaces $\Gamma_1 \cup \Gamma_2$. The flux continuity is instead a consequence of the fact that the test functions ϕ_i are also equal along these surfaces. In this way, the boundary terms along $\Gamma_1 \cup \Gamma_2$ can only vanish if the outwards normal components of the fluxes cancel each other.

The numerical iterative scheme considered here also provides proof for the existence of the time-discrete formulation. Moreover, one can treat more complicated reaction rates (for example, Lipschitz reaction rates) by considering Euler explicit time stepping in the reaction term. For numerical reasons, we formulate the original problem in the three (non-overlapping) domains. This allows separating the computations at the trench scale from those at the reactor scale without requiring any correlation between the meshes employed at the different scales. Having introduced the weak solutions above, we now consider a numerical scheme for computing the solution at each time step and investigate its convergence. To simplify the presentation we fix a time step t_k and define

$$v_i := u_i^k, \quad i = 1, 2, 3,$$

so that all the estimates are obtained in terms of v_i.

4.2. The iterative domain decomposition scheme

Here we describe the iterative scheme used for solving the time-discrete problem (4.2). The scheme is inspired from [4,7]. To understand its background, we consider first the strong form of the equation and define the quantities ($\boldsymbol{\nu}_1$ is the normal to Γ_1 and into Ω_1; $\boldsymbol{\nu}_2$ is normal to Γ_2 and into Ω_2)

$$g_{21} := \boldsymbol{\nu}_1 \cdot (-\nabla v_2) + \lambda v_2 \quad \text{and} \quad g_{12} := \boldsymbol{\nu}_1 \cdot \nabla v_1 + \lambda v_1 \quad \text{on } \Gamma_1, \tag{4.3}$$

$$g_{23} := \boldsymbol{\nu}_2 \cdot \nabla v_2 + \lambda v_2 \quad \text{and} \quad g_{32} := -\boldsymbol{\nu}_2 \cdot (D_T \nabla v_3) + \lambda v_3 \quad \text{on } \Gamma_2, \tag{4.4}$$

where $\lambda > 0$ is a positive constant. For the convergence proof, it suffices to have $\lambda > 0$; however, its value influences the speed of convergence [8]. Note that the g_{ij} terms depend on the time step k and define (decoupling) boundary conditions at the non-reacting interfaces. To ensure that solving the decoupled problems provides a solution of the originally coupled one, additional conditions will be given later.

Before constructing the nth iterate, we remark on the following notation used here. By $g_{ji} \in H^{1/2}$ we imply that $\{g_{12}, g_{21}\} \in H^{1/2}(\Gamma_1)$ and $\{g_{23}, g_{32}\} \in H^{1/2}(\Gamma_2)$. On the basis of the above we let $n \in \mathbb{N}$ denote the iteration index and construct the nth iterate as the solution of:

Problem $\mathbf{P}^n$. Given $v_i^{n-1} \in H^1_{0,\Gamma_D}(\Omega_i)$ and $g_{ji}^{n-1} \in H^{1/2}$ $(i, j = 1, 2, 3, |i-j| = 1)$, find $v_i^n \in H^1_{0,\Gamma_D}(\Omega_i)$ such that

$$\frac{1}{\triangle t}(v_1^n, \phi_1)_{\Omega_1} + (\nabla v_1^n, \nabla\phi_1)_{\Omega_1} + (C_R v_1^n, \phi_1)_{\Gamma_{1R}} + (g_{12}^n, \phi_1)_{\Gamma_1} = \frac{1}{\triangle t}(u_1^{k-1}, \phi_1)_{\Omega_1} - (\mathbf{q}\nabla u_1^{k-1}, \phi_1)_{\Omega_1}, \tag{4.5}$$

$$\frac{1}{\triangle t}(v_2^n, \phi_2)_{\Omega_2} + (\nabla v_2^n, \nabla\phi_2)_{\Omega_2} + (C_R v_2^n, \phi_2)_{\Gamma_{2R}} + (g_{21}^n, \phi_2)_{\Gamma_1} + (g_{23}^n, \phi_2)_{\Gamma_2}$$
$$= \frac{1}{\triangle t}(u_2^{k-1}, \phi_2)_{\Omega_2} - (\mathbf{q}\nabla u_2^{k-1}, \phi_2)_{\Omega_2}, \tag{4.6}$$

$$\frac{1}{\triangle t}(v_3^n, \phi_3)_{\Omega_3} + (D_T\nabla v_3^n, \nabla\phi_3)_{\Omega_3} + (C_R v_3^n, \phi_3)_{\Gamma_{3R}} + (g_{32}^n, \phi_3)_{\Gamma_2} = \frac{1}{\triangle t}(u_3^{k-1}, \phi_3)_{\Omega_3} \tag{4.7}$$

for all $\phi_i \in H^1_{0,\Gamma_D}(\Omega_i)$, such that $\phi_1 = \phi_2$ on Γ_1 and $\phi_2 = \phi_3$ on Γ_2. Furthermore, for g_{ij}, $|i-j| = 1$, the update takes place according to

$$g_{ij}^n := 2\lambda v_j^{n-1} - g_{ji}^{n-1}. \tag{4.8}$$

The iterative scheme requires a starting triple (v_1^0, v_2^0, v_3^0). Since the problem under consideration is, in fact, an evolution one, a good option is $v_i^0 = u_i^{k-1}$. However, this choice is not required for the convergence proof below. Also, with $u_i^{k-1} \in H^1_{0,\Gamma_D}$, the initial datum for g_{ij} need not be in $H^{1/2}_{\Gamma_1/\Gamma_2}$. Therefore, to start the iteration, we choose $g_{ij}^0 = -\boldsymbol{\nu}\cdot\nabla v_i^0 + \lambda v_i^0$ for $i \neq 3$; and $g_{32}^0 = -\boldsymbol{\nu}\cdot D_T\nabla v_3^0 + \lambda v_3^0$ whenever u_i^{k-1} has sufficient regularity, and otherwise smooth it by convolution to ensure that $g_{ij}^0 \in H^{1/2}_{\Gamma_1/\Gamma_2}$. For the notation, we recall that k is the time step and n stands for the iteration index. Thus v_i^n stands for $u_i^{k,n}$, the nth iterate at time step $t = t_k$. Note that at each iterative step n, the equations are decoupled by the boundary conditions obtained from the previous iterative step. Furthermore, the indices i, j refer to the enumeration of subdomains.

Remark 4.1. As stated earlier in the definition of Problem $\mathbf{P}^n$, we assume that $u_i^{k-1} \in H^1_{0,\Gamma_D}(\Omega_i)$. Moreover, choosing the initial data, by smoothing if necessary, we have $g_{ij}^0 \in H^{1/2}_{\Gamma_1/\Gamma_2}$. With the boundary conditions decoupled for the Problem $\mathbf{P}^n$, the standard elliptic theory provides existence and uniqueness of the solution triple v_i^n.

Remark 4.2. Note that the explicit discretization of the convective term requires the CFL condition to be satisfied for stability reasons. This may seem restrictive especially in view of spatial discretization of Ω_2 being much smaller compared to the macroscale discretization. However, note that with the parabolic inlet profile of the fluid velocity (and no-slip boundary condition), $\mathbf{q}$ itself is much smaller in Ω_2, in fact of the order of $|\Omega_2|$. Thus, the CFL restriction is quite reasonable with

$$\triangle t \leq \min\left\{\frac{h_2}{Q|\Omega_2|}, \frac{h_1}{Q}\right\}$$

where h_1 and h_2 refer to the sizes of spatial discretization of Ω_1 and Ω_2, respectively.

Before giving a rigorous convergence proof, we give a formal justification of the iterative scheme. Assuming that $v_i^n \to v_i$ and $g_{ij}^n \to g_{ij}$, passing to the limit in the updates (4.8) gives

$$g_{ij} = 2\lambda v_j - g_{ji}.$$

In other words, at Γ_1 we have

$$g_{12} = 2\lambda v_2 - g_{21}, \quad \text{and} \quad g_{21} = 2\lambda v_1 - g_{12},$$

implying $v_2 = v_1$. Once the continuity is established, the following simple calculation establishes the equality of the normal components of the diffusive fluxes at Γ_1:

$$\boldsymbol{\nu}_1\cdot\nabla v_1 - \boldsymbol{\nu}_1\cdot\nabla v_2 + \lambda(v_1 + v_2) = g_{12} + g_{21} = 2\lambda v_1 = \lambda(v_1 + v_2).$$

The justification of the coupling conditions at Γ_2 is completely similar.

In the formal definition of g_{ij} above, we have only included the normal diffusive fluxes. This is because equality of the normal components of the diffusive fluxes together with the continuity of concentration also implies the equality of the normal fluxes. Clearly,

$$\boldsymbol{\nu}_1\cdot(-\nabla u_2 + \mathbf{q}u_2) = \boldsymbol{\nu}_1\cdot(-\nabla u_1 + \mathbf{q}u_1) \quad \text{on } \Gamma_1$$

and similarly for Γ_2.

4.3. The convergence proof

We follow the ideas in [4], and the main ideas of the proof are obtaining a priori estimates for v_i^n and using compactness arguments to show the H^1 convergence in space. Application of compact embeddings and trace inequalities leads to establishing convergence on the boundaries. It is subsequently not particularly difficult to prove that the limits satisfy the time-discrete formulation (4.2).

We have the following theorem:

Theorem 4.1. *As $n \to \infty$, the solutions v_i^n satisfying (4.5)–(4.7) converge weakly in $H^1(\Omega_i)$ to v_i satisfying (4.2).*

4.3.1. A priori estimates

To prepare the proof of Theorem 4.1, we define the following:

$$e_i^n := v_i^n - v_i^{n-1} \quad (i = 1, 2, 3), \tag{4.9}$$

$$e_{1,\Gamma_1}^n := g_{12}^n - g_{12}^{n-1}, \qquad e_{2,\Gamma_1}^n = g_{21}^n - g_{21}^{n-1}, \tag{4.10}$$

$$e_{3,\Gamma_2}^n := g_{32}^n - g_{32}^{n-1}, \qquad e_{4,\Gamma_2}^n = g_{23}^n - g_{32}^{n-1}, \tag{4.11}$$

$$e_{\Gamma_1}^n := \left[(e_{1,\Gamma_1}^n)^2 + (e_{2,\Gamma_2}^n)^2\right]^{1/2}, \qquad e_{\Gamma_2}^n := \left[(e_{3,\Gamma_2}^n)^2 + (e_{4,\Gamma_2}^n)^2\right]^{1/2}. \tag{4.12}$$

With these definitions in mind, we have the following lemma.

Lemma 4.1. *A constant $C > 0$ depending on the starting triple (v_1^0, v_2^0, v_3^0) exists such that the boundary errors introduced in (4.9) satisfy*

$$\sum_{n=1}^{N} \left(\|e_1^n\|_{\Gamma_1}^2 + \|e_2^n\|_{\Gamma_1}^2 + \|e_2^n\|_{\Gamma_2}^2 + \|e_3^n\|_{\Gamma_2}^2\right) \le C. \tag{4.13}$$

Proof. Subtracting (4.5) for v_1^{n-1} from the one for v_1^n gives

$$\begin{aligned}&\frac{1}{\triangle t}(v_1^n - v_1^{n-1}, \phi_1)_{\Omega_1} + (\nabla v_1^n - \nabla v_1^{n-1}, \nabla\phi_1)_{\Omega_1} + C_R(v_1^n - v_1^{n-1}, \phi_1)_{\Gamma_{1R}} \\ &\quad + \lambda(v_1^n - v_1^{n-1}, \phi_1)_{\Gamma_1} - (g_{12}^n - g_{12}^{n-1}, \phi_1)_{\Gamma_1} = 0.\end{aligned} \tag{4.14}$$

Taking in the above $\phi_1 = e_1^n$ leads to

$$\frac{1}{\triangle t}\|e_1^n\|_{\Omega_1}^2 + \|\nabla e_1^n\|_{\Omega_1}^2 + C_R\|e_1^n\|_{\Gamma_{1R}}^2 + \lambda\|e_1^n\|_{\Gamma_1}^2 = (e_{1,\Gamma_1}^n, e_1^n)_{\Gamma_1}. \tag{4.15}$$

In a similar manner one gets

$$\frac{1}{\triangle t}\|e_2^n\|_{\Omega_2}^2 + \|\nabla e_2^n\|_{\Omega_2}^2 + C_R\|e_2^n\|_{\Gamma_{2R}}^2 + \lambda\|e_2^n\|_{\Gamma_1}^2 + \lambda\|e_2^n\|_{\Gamma_2}^2 = (e_{2,\Gamma_1}^n, e_2^n)_{\Gamma_1} + (e_{3,\Gamma_2}^n, e_3^n)_{\Gamma_2}, \tag{4.16}$$

and

$$\frac{1}{\triangle t}\|e_3^n\|_{\Omega_3}^2 + \|D_T\nabla e_3^n\|_{\Omega_3}^2 + C_R\|e_3^n\|_{\Gamma_{3R}}^2 + \lambda\|e_3^n\|_{\Gamma_2}^2 = (e_{4,\Gamma_2}^n, e_3^n)_{\Gamma_2}. \tag{4.17}$$

Recalling the notation in (4.10)–(4.12), we have

$$\begin{aligned}(e_{\Gamma_1}^{n+1})^2 &= (g_{12}^{n+1} - g_{12}^n)^2 + (g_{21}^{n+1} - g_{21}^n)^2 \\ &= (2\lambda(v_2^n - v_2^{n-1}) - g_{21}^n + g_{21}^{n-1})^2 + (2\lambda(v_1^n - v_1^{n-1}) - g_{12}^n + g_{12}^{n-1})^2 \\ &= (2\lambda(v_2^n - v_2^{n-1}) - e_{2,\Gamma_1}^n)^2 + (2\lambda(v_1^n - v_1^{n-1}) - e_{1,\Gamma_1}^n) \\ &= (e_{1,\Gamma_1}^n)^2 + (e_{2,\Gamma_1}^n)^2 + 4\lambda(\lambda(v_1^n - v_1^{n-1}) - e_{1,\Gamma_1}^n)(v_1^n - v_1^{n-1}) + 4\lambda(\lambda(v_2^n - v_2^{n-1}) - e_{2,\Gamma_1}^n)(v_2^n - v_2^{n-1}).\end{aligned}$$

By (4.12) this gives

$$(e_{\Gamma_1}^{n+1})^2 - (e_{\Gamma_1}^n)^2 = 4\lambda(\lambda e_1^n - e_{1,\Gamma_1}^n, e_1^n)_{\Gamma_1} + 4\lambda(\lambda e_2^n - e_{2,\Gamma_1}^n, e_2^n)_{\Gamma_1}.$$

Similarly,

$$(e_{\Gamma_2}^{n+1})^2 - (e_{\Gamma_2}^n)^2 = 4\lambda(\lambda e_2^n - e_{3,\Gamma_2}^n, e_2^n)_{\Gamma_2} + 4\lambda(\lambda e_3^n - e_{4,\Gamma_2}^n, e_3^n)_{\Gamma_2}.$$

With the above, adding (4.15)–(4.17) gives

$$\frac{1}{\triangle t}\|e_1^n\|^2_{\Omega_1} + \|\nabla e_1^n\|^2_{\Omega_1} + C_R(\|e_1^n\|^2_{\Gamma_{1R}} + \|e_2^n\|^2_{\Gamma_{2R}} + \|e_3^n\|^2_{\Gamma_{3R}}) + \frac{1}{\triangle t}\|e_2^n\|^2_{\Omega_2} + \|\nabla e_2^n\|^2_{\Omega_2}$$
$$+ \frac{1}{\triangle t}\|e_3^n\|^2_{\Omega_3} + \|\nabla e_3^n\|^2_{\Omega_3} + \frac{1}{4\lambda}\left(\|e_{\Gamma_1}^{n+1}\|^2_{\Gamma_1} - \|e_{\Gamma_1}^n\|^2_{\Gamma_1}\right) + \frac{1}{4\lambda}\left(\|e_{\Gamma_1}^{n+1}\|^2_{\Gamma_2} - \|e_{\Gamma_2}^n\|^2_{\Gamma_2}\right) = 0.$$

Summing the above over $n = 1 \cdots N$ leads to

$$\|e_{\Gamma_1}^{N+1}\|^2 + \|e_{\Gamma_2}^{N+1}\|^2 + 4\lambda \sum_{n=1}^{N}\left(\|\nabla e_1^n\|^2 + \|\nabla e_2^n\|^2 + \|\nabla e_3^n\|^2\right)$$
$$+ \frac{4\lambda}{\triangle t}\sum_{n=1}^{N}\left(\|e_1^n\|^2_{\Omega_1} + \|e_2^n\|^2_{\Omega_2} + \|e_3^n\|^2_{\Omega_3}\right) + C_R(\|e_1^n\|^2_{\Gamma_{1R}} + \|e_2^n\|^2_{\Gamma_{2R}} + \|e_3^n\|^2_{\Gamma_{3R}}) = \|e_{\Gamma_1}^0\|^2_{\Gamma_1} + \|e_{\Gamma_2}^0\|^2_{\Gamma_2}. \tag{4.18}$$

By assumptions on the initial data, one has $\|e^0_{\Gamma_1}\|_{\Gamma_1} + \|e^0_{\Gamma_2}\|^2_{\Gamma_2} \le C$ (C depends on the initial datum). An application of the trace theorem in view of the above inequality gives

$$\sum_{n=1}^{N}\left(\|e_1^n\|^2_{\Gamma_1} + \|e_2^n\|^2_{\Gamma_1} + \|e_2^n\|^2_{\Gamma_2} + \|e_3^n\|^2_{\Gamma_2}\right) \le C, \tag{4.19}$$

which concludes the proof. □

Lemma 4.1 implies that the series on the left of (4.13) is finite; therefore the (error) terms are converging to 0. However, this is not sufficient for proving the desired convergence result.

Lemma 4.2. *With the solution triple* (v_1^n, v_2^n, v_3^n) *solving Problem* $\mathbf{P}^n$ $(n \ge 1)$, *one has*

$$\sum_{i=1}^{3}\|v_i^N\|^2_{H^1(\Omega_i)} + \sum_{n=1}^{N}\left(\|v_1^{n+1} - v_2^n\|^2_{\Gamma_1} + \|v_2^{n+1} - v_1^n\|^2_{\Gamma_1} + \|v_1^{n+1} - v_3^n\|^2_{\Gamma_2} + \|v_3^{n+1} - v_2^n\|^2_{\Gamma_2}\right) \le C \tag{4.20}$$

with C *independent of* N *and depending on the initial data.*

Proof. We start by observing that

$$g_{12}^{n+1} - g_{12}^{n-1} = 2\lambda v_2^n - 2\lambda v_1^{n-1}, \qquad g_{21}^{n+1} - g_{21}^{n-1} = 2\lambda v_1^n - 2\lambda v_2^{n-1},$$
$$g_{23}^{n+1} - g_{23}^{n-1} = 2\lambda v_3^n - 2\lambda v_2^{n-1}, \qquad g_{32}^{n+1} - g_{32}^{n-1} = 2\lambda v_2^n - 2\lambda v_3^{n-1}.$$

Further, we have the elementary identities

$$(v_i^{n+1} - v_i^{n-1}, v_i^{n+1}) = \frac{1}{2}\|v_i^{n+1}\|^2 + \frac{1}{2}\|v_i^{n+1} - v_i^{n-1}\|^2 - \frac{1}{2}\|v_i^{n-1}\|^2,$$
$$(\nabla(v_i^{n+1} - v_i^{n-1}), \nabla v_i^{n+1}) = \frac{1}{2}\|\nabla v_i^{n+1}\|^2 + \frac{1}{2}\|\nabla(v_i^{n+1} - v_i^{n-1})\|^2 - \frac{1}{2}\|\nabla v_i^{n-1}\|^2,$$
$$(v_i^{n+1} + v_i^{n-1} - 2v_j^n, v_i^{n+1}) = \frac{1}{2}\|v_i^{n+1}\|^2 + \frac{1}{2}\|v_i^{n-1}\|^2 - \|v_j^n\|^2 + \|v_i^{n+1} - v_j^n\|^2 - \frac{1}{2}\|v_i^{n+1} - v_i^{n-1}\|^2.$$

We now proceed as in Lemma 4.1 and subtract (4.5)–(4.7) for v_i^{n-1} from the one for v_i^{n+1}, test the resulting with $\phi = v_i^{n+1}$, and double the result and sum it over $n = 1, \ldots, N$ to obtain

$$\frac{1}{\triangle t}\sum_{i=1}^{3}\left(\|v_i^{N+1}\|^2_{\Omega_1} + \|v_i^N\|^2_{\Omega_1}\right) + \sum_{i=1}^{3}\left(\|\nabla v_i^{N+1}\|^2_{\Omega_1} + \|\nabla v_i^N\|^2_{\Omega_1}\right)$$
$$+ \frac{1}{\triangle t}\sum_{n=1}^{N}\sum_{i=1}^{3}\|v_i^{n+1} - v_i^{n-1}\|^2_{\Omega_i} + \sum_{n=1}^{N}\sum_{i=1}^{3}\|\nabla v_i^{n+1} - \nabla v_i^{n-1}\|^2_{\Omega_i}$$
$$+ \sum_{i=1}^{3}\left(\|v_i^{N+1}\|^2_{\Gamma_{iR}} + \|v_i^N\|^2_{\Gamma_{iR}} + \sum_{n=1}^{N}\|v_i^{n+1} - v_i^{n-1}\|^2_{\Gamma_{iR}}\right)$$
$$+ 2\sum_{n=1}^{N}\left(\|v_1^{n+1} - v_2^n\|^2_{\Gamma_1} + \|v_2^{n+1} - v_1^n\|^2_{\Gamma_1} + \|v_2^{n+1} - v_3^n\|^2_{\Gamma_2} + \|v_3^{n+1} - v_2^n\|^2_{\Gamma_2}\right)$$
$$\le C + \sum_{n=1}^{N}\left(\|v_1^{n+1} - v_1^{n-1}\|_{\Gamma_1} + \|v_2^{n+1} - v_2^{n-1}\|_{\Gamma_1} + \|v_2^{n+1} - v_2^{n-1}\|_{\Gamma_2} + \|v_3^{n+1} - v_3^{n-1}\|_{\Gamma_2}\right).$$

Using (4.19) in the above yields

$$\sum_{i=1}^{3}\left(\|v_i^N\|_{\Omega_i}^2+\|\nabla v_i^N\|_{\Omega_i}^2\right)+\sum_{n=1}^{N}\left(\|v_1^{n+1}-v_2^n\|_{\Gamma_1}^2+\|v_2^{n+1}-v_1^n\|_{\Gamma_1}^2+\|v_1^{n+1}-v_3^n\|_{\Gamma_2}^2+\|v_3^{n+1}-v_2^n\|_{\Gamma_2}^2\right)\le C \tag{4.21}$$

with C independent of N and depending only on the initial data. □

4.3.2. Proof of Theorem 4.1

Proof. Lemma 4.2 provides enough compactness for passing to the limit. Note that (4.21) implies that there exists a subsequence again denoted by v_i^n such that

$$v_i^n \to v_i \quad \text{weakly in } H^1(\Omega_i)$$

and, hence, strongly in $L^2(\Omega_i)$. Further, to establish the continuity of the concentration at the boundaries, let us take, for instance,

$$\|v_1-v_2\|_{\Gamma_1}\le\|v_1-v_1^{n+1}\|_{\Gamma_1}+\|v_2^{n+1}-v_2\|_{\Gamma_1}+\|v_1^{n+1}-v_2^{n+1}\|_{\Gamma_1}$$

whereby the last term on the right hand side vanishes because of estimate (4.21). The vanishing of the first two terms is a consequence of the weak convergence in H^1 leading to L^2 strong convergence at the boundaries. Similarly, $v_2=v_3$ at the boundary Γ_2.

From the preceding discussions, we conclude that the triple $(v_1, v_2, v_3)\equiv(u_1^k, u_2^k, u_3^k)$ satisfies

$$\begin{aligned}&\frac{1}{\triangle t}(u_1^k-u_1^{k-1},\phi_1)_{\Omega_1}+(\nabla u_1^k,\nabla\phi_1)_{\Omega_1}-(\mathbf{q}\nabla u_1^{k-1},\phi_1)_{\Omega_1}\\&\quad+(C_R u_1^k,\phi_1)_{\Gamma_{1R}}+\frac{1}{\triangle t}(u_2^k-u_2^{k-1},\phi_2)_{\Omega_2}+(\nabla u_2^k,\nabla\phi_2)_{\Omega_2}-(\mathbf{q}\nabla u_2^{k-1},\phi_2)_{\Omega_2}\\&\quad+(C_R u_2^k,\phi_2)_{\Gamma_{2R}}+\frac{1}{\triangle t}(u_3^k-u_3^{k-1},\phi_3)_{\Omega_3}+(D_T\nabla u_3^k,\nabla\phi_3)_{\Omega_3}+(C_R u_3^k,\phi_3)_{\Gamma_{3R}}=0\end{aligned} \tag{4.22}$$

for all $\phi_i\in H^1(\Omega_i)$ such that $\phi_1=\phi_2$ at Γ_1 and $\phi_2=\phi_3$ at Γ_2. □

Acknowledgments

The work of K. Kumar was supported by STW project No. 07796. The support is gratefully acknowledged. We would also like to thank the anonymous referees for their careful reading and constructive suggestions.

References

[1] P.H.L. Notten, F. Roozeboom, R.A.H. Niessen, L. Baggetto, 3-d integrated all-solid-state rechargeable batteries, Advanced Materials 19 (2007) 4564–4567.
[2] J.F.M. Oudenhoven, L. Bagetto, P.H.L. Notten, All-solid-state lithium-ion microbatteries: a review of various three-dimensional concepts, Advanced Energy Materials 1 (2011) 10–33.
[3] J.F.M. Oudenhoven, T. van Dongen, R.A.H. Niessen, M.H.J.M. de Croon, P.H.L. Notten, Low-pressure chemical vapor deposition of $LiCoO_2$ thin films: A systematic investigation of the deposition parameters, Journal of the Electrochemical Society 156 (2009) D159–D174.
[4] P.L. Lions, On the Schwarz alternating method. I, in: First International Symposium on Domain Decomposition Methods for Partial Differential Equations (Paris, 1987), SIAM, Philadelphia, PA, 1988, pp. 1–42.
[5] C. Cancès, M. Pierre, An existence result for multidimensional immiscible two-phase flows with discontinuous capillary pressure field, SIAM Journal on Mathematical Analysis 44 (2012) 966–992.
[6] W. Jäger, N. Kutev, Discontinuous solutions of the nonlinear transmission problem for quasilinear elliptic equations. Preprint IWR Universität Heidelberg IWR, 98-22 (SFB 359), 1998, pp. 1–37.
[7] P.L. Lions, On the Schwarz alternating method. III. a variant for nonoverlapping subdomains, in: Third International Symposium on Domain Decomposition Methods for Partial Differential Equations (Houston, TX, 1989), SIAM, Philadelphia, PA, 1990, pp. 202–223.
[8] J. Bogers, Well-posedness, upscaling and numerical schemes for problems involving a nonlinear transmission condition, Masters Thesis, Technische Universiteit Eindhoven, 2011, pp. 100–101.